Journal of Mechanical Design. Received August 19, 2021;
Accepted manuscript posted November 30, 2021. doi:10.1115/1.4053217

Final Paper to ASME Journal of Mechanical Design

Reliability-Based Multi-Vehicle Path Planning Under Uncertainty Using a Bio-Inspired Approach

Yixuan Liu[1], Chen Jiang[1], Xiaoge Zhang[2], Zissimos P. Mourelatos[3], Dakota Barthlow[3], David Gorsich[4], Amandeep Singh[4], and Zhen Hu[1*]

[1]Department of Industrial and Manufacturing Systems Engineering, University of Michigan-Dearborn, Dearborn, MI 48128, USA
[2]Department of Industrial and Systems Engineering, The Hong Kong Polytechnic University, Hung Hom, Kowloon, Hong Kong
[3]Mechanical Engineering Department, Oakland University, Rochester, MI 48309, USA
[4]US Army Combat Capabilities Development Command, Ground Vehicle Systems Center, Warren, MI 48397, USA

* Corresponding author: 2340 HPEC, University of Michigan-Dearborn, Dearborn, MI 48128, USA, Tel:+1-313-583-6312, Email: zhennhu@umich.edu

Journal of Mechanical Design. Received August 19, 2021;
Accepted manuscript posted November 30, 2021. doi:10.1115/1.4053217

AUTHORS INFORMATION:

Yixuan Liu

Ph.D. student

Department of Industrial and Manufacturing Systems Engineering,

University of Michigan-Dearborn,

2340 Heinz Prechter Engineering Complex,

Dearborn, MI, 48128

E-mail: yixuanli@umich.edu

Chen Jiang

Postdoctoral Research Scholar

Department of Industrial and Manufacturing Systems Engineering,

University of Michigan-Dearborn,

2340 Heinz Prechter Engineering Complex,

Dearborn, MI, 48128

E-mail: chejiang@umich.edu

Xiaoge Zhang

Assistant Professor

Department of Industrial and Systems Engineering

The Hong Kong Polytechnic University

Hung Hom, Kowloon, Hong Kong

E-mail: xiaoge.zhang@polyu.edu.hk

Zissimos P. Mourelatos

Distinguished University Professor

Mechanical Engineering Department,

Oakland University,

Engineering Center, Room 402D, 115 Library Drive,

Rochester, MI, 48309

E-mail: mourelat@oakland.edu

Journal of Mechanical Design. Received August 19, 2021;
Accepted manuscript posted November 30, 2021. doi:10.1115/1.4053217

Dakota Barthlow
Ph.D. student
Mechanical Engineering Department,
Oakland University,
Engineering Center, Room 402D, 115 Library Drive,
Rochester, MI, 48309
E-mail: drbarthlow@oakland.edu

David Gorsich
Chief Scientist
U.S. Army Combat Capabilities Development Command,
Ground Vehicle Systems Center,
6501 E. 11 Mile Road,
Warren, MI 48397
E-mail: david.j.gorsich.civ@mail.mil

Amandeep Singh
Branch Chief
U.S. Army Combat Capabilities Development Command,
Ground Vehicle Systems Center,
6501 E. 11 Mile Road,
Warren, MI 48397
E-mail: david.j.gorsich.civ@mail.mil

Zhen Hu
Corresponding Author
Assistant Professor
Department of Industrial and Manufacturing Systems Engineering,
University of Michigan-Dearborn,
2340 Heinz Prechter Engineering Complex,
Dearborn, MI, 48128
E-mail: zhennhu@umich.edu

Journal of Mechanical Design. Received August 19, 2021;
Accepted manuscript posted November 30, 2021. doi:10.1115/1.4053217

ABSTRACT

Identifying a reliable path in uncertain environments is essential for designing reliable off-road autonomous ground vehicles (AGV) considering post-design operations. This paper presents a novel bio-inspired approach for model-based multi-vehicle mission planning under uncertainty for off-road AGVs subjected to mobility reliability constraints in dynamic environments. A physics-based vehicle dynamics simulation model is first employed to predict vehicle mobility (i.e., maximum attainable speed) for any given terrain and soil conditions. Based on physics-based simulations, the vehicle state mobility reliability in operation is then analyzed using an adaptive surrogate modeling method to overcome the computational challenges in mobility reliability analysis by adaptively constructing a surrogate. Subsequently, a bio-inspired approach called Physarum-based algorithm is used in conjunction with a navigation mesh to identify an optimal path satisfying a specific mobility reliability requirement. The developed Physarum-based framework is applied to reliability-based path planning for both a single-vehicle and multiple-vehicle scenarios. A case study is used to demonstrate the efficacy of the proposed methods and algorithms. The results show that the proposed framework can effectively identify optimal paths for both scenarios of a single and multiple vehicles. The required computational time is less than the widely used Dijkstra-based method.

Keywords: Mobility reliability, Path planning, Simulation, Physarum algorithm

1 INTRODUCTION

Off-road autonomous ground vehicles (AGVs) and other types of robotics are drawing increased attention in recent years as they are able to work in dangerous situations such as wildfires or earthquakes [1], and replace humans in fields such as agricultural and battlefield [2]. The design of reliable autonomous engineering systems, such as off-road AGVs studied in this paper, is a challenging issue since it must consider post-design autonomous operations (e.g. path/mission planning or re-planning) to guarantee the reliability of the system during operation.

One of the most important aspects in design of reliable AGVs considering post-design operations is mission planning (also called path planning). For a given vehicle design, a properly planned path using model-based approach will help the AGV to better accomplish the mission in the post-design stage with higher speed [3], lower energy consumption [4], and higher reliability [5]. The goal of this paper is to develop a model-based mission planning framework to guarantee the reliability of AGV operation in the early design stage. As shown in Fig.1, a proper model-based off-road mission planning process mainly consists of two phases: (1) *transforming the target map into a vehicle mobility map* using the target map information and the off-road mobility predictive model, and (2) *finding the optimal path* under predefined mission requirements based on the vehicle mobility map.

In the *first* phase, the first step is to build a simulation-based mobility predictive model to predict vehicle mobility in items of speed, acceleration, or energy consumption for the off-road AGVs. In the past decades, many off-road mobility models, such as the NATO Reference Mobility Model (NRMM) [6, 7], the next-generation NRMM (NG-NRMM) [8, 9], the physics-based deformable tire–soil interaction model [10], and the Bekker's derived terramechanics model (BDTM) [11], have been developed to predict the vehicle dynamic performance under

Journal of Mechanical Design. Received August 19, 2021;
Accepted manuscript posted November 30, 2021. doi:10.1115/1.4053217

different conditions. Plugging the terrain-related parameters associated with a target map and the vehicle-related parameters into the mobility predictive model enables the generation of a vehicle mobility map, which provides the vehicle performance prediction, in terms of the mean maximum pressure (MMP) [12] or the maximum vehicle speed of the vehicle at each location [13].

Place Figure 1 here

Since the terrain-related parameters (e.g., terrain slope and soil properties) are not constants but vary due to weather variations for example, the obtained vehicle mobility at each spatial location is uncertain. To consider the uncertainty in the vehicle mobility prediction, many methods have been developed. For instance, Haug et al. [14] described the domain of mobility when an object is moving in an area with obstacles. Gonzalez et al. [13, 15] developed a geostatistical approach to predict the off-road mobility and generate a mobility map over a large area. Choi et al. [16] proposed a framework to construct a reliability-based stochastic mobility map. Jayakumar et al. [17] built a method to generate a mobility map using machine learning algorithms such as support vector machines and neural networks. Hu et al. [18] established a testing design optimization approach to reduce the uncertainty when generating the mobility map.

In the *second* phase, many approaches have been proposed to determine an optimal path for off-road vehicles by using the mobility information and considering the uncertainty or risk associated with the area of the mission. For instance, Yang [19] proposed a Nonperiodic B-Spline Curves-based path planning approach for autonomous robots or vehicles to avoid obstacles in the mission area. Rapidly-exploring random trees (RRT) has been used for path

planning considering uncertainty in the terrain [20]. Liu et al. [1] proposed an A-star based approach to find a robust path in complex off-road environment. Sun et al. [21] introduced a stochastic extended linear quadratic regulator (SELQR) approach by minimizing the expected value of a user-defined cost function and modeling the uncertainty with a Gaussian distribution. A linear-quadratic Gaussian motion planning (LQG-MP) with RRT has been developed by Berg [22] to generate a proper path under Gaussian uncertainty. Zhang et al. [23] proposed a geometric reinforcement learning algorithm for path planning by considering risk in the reward matrix. Chao et al. [24] introduced a grid-based RRT* approach that provides a path with minimum risk in the dangerous area. Moreover, in order to consider the dependence of the uncertain terrain-related parameters over the target map, Jiang et al. [5] proposed a R2-RRT* method by combining a state mobility reliability (space independent) and mission mobility reliability (space dependent)) to identify an optimal path satisfying a required mission reliability level [25].

Although the existing approaches have achieved acceptable results in finding the optimal mission path, there are still some limitations. First, some approaches used empirical models instead of high-fidelity multi-body dynamic models to predict vehicle mobility in off-road conditions, which could lead to large errors in the vehicle mobility prediction. Some other approaches used a certain type of high-fidelity vehicle dynamic models as the mobility predictive model, which is computationally very costly and is not suitable for model-based mission planning in uncertain off-road environment. Secondly, even though mission planning for an unmanned aerial vehicle (UAV) swarm has been widely studied [26-28], multi-vehicle model-based mission planning for off-road AGVs has been rarely studied. Also, if the map is not properly represented, it will increase the computational effort and calculation time which is undesirable in dynamic missing planning in changing environment.

Journal of Mechanical Design. Received August 19, 2021;
Accepted manuscript posted November 30, 2021. doi:10.1115/1.4053217

To overcome the aforementioned limitations, we proposed a novel path planning approach based on a bio-inspired Physarum-based algorithm. We first use an open-source high-fidelity dynamic simulation model named PyChrono to predict vehicle mobility in uncertain off-road environment [29]. To overcome the computational challenge in mobility prediction uncertainty caused by the PyChrono simulations, we employ an adaptive surrogate modeling method to construct an efficient and yet accurate surrogate model of the original mobility simulation model. The constructed surrogate model is then used to generate a probabilistic vehicle mobility map by considering various uncertainty sources in the terrain and soil parameters. After that, we transform the original mobility map into a navigation map using a navigation mesh to further reduce the computational time in mission planning by reducing the nodes and edges in a network used to represent the map. Finally, we develop single vehicle and multi-vehicle path planning subjected to a reliability constraint using a novel Physarum-based algorithm. The main contributions of this paper are summarized as: (1) a systematic reliability-based multi-vehicle mission planning framework is developed for AGVs in uncertain off-road environments using model-based approach in the early design; (2) synthesis of an adaptive surrogate modeling method and a navigation mesh is used to drastically reduce the computational time in reliability-based mission planning; and (3) a novel bio-inspired Physarum algorithm is used to efficiently perform multi-vehicle mission planning in a dynamic environment. Even though the proposed method is demonstrated using an off-road AGV, it is also applicable to path planning of unmanned aerial vehicles in uncertain environment.

The remainder of this paper is organized as follows. Section 2 describes the off-road mobility model and the off-road mission planning. Section 3 introduces the proposed Physarum-based approach. Section 4 uses a case study to demonstrate the proposed algorithms. Finally, Section 5 draws conclusions.

2 BACKGROUND

2.1 Off-Road Vehicle Mobility Analysis Model

Although many approaches have been developed in the past decades, it is still a challenging issue to accurately predict the off-road mobility of an AGV due to the complex physical interactions between the vehicle and terrain [30], especially for deformable terrain conditions. For example, Rubinstein et al. [31] developed a detailed multi-body dynamic simulation model for tracked off-road vehicles. Liang et al. [32] proposed a semi-empirical approach of tire modeling to simulate the tire/terrain interaction. Krenn et al. [33] combined soft soil contact models with Bekker's terramechanics theory to create an efficient approach for multi-body dynamic simulation. Senatore et al. [34] used rigid wheels and flexible tires to build a tire model for off-road dynamic simulation.

In this paper, the open source multi-physics simulation package, PyChrono [35, 36], is employed to predict vehicle mobility for any given terrain/soil conditions and to generate a vehicle mobility map (Phase 1 in Fig. 1). PyChrono is the Python version of Chrono which is programmed in C++. The advantages of PyChrono are that it is simple to use and to be combined with other python libraries. More specifically, the Pychrono: Vehicle module is used in this paper. It provides different types of vehicles running on a rigid, granular, or deformable terrain. A driving vehicle controller can also be used for closed-loop or interactive vehicle behavior control. Fig. 2 shows two simulation examples in PyChrono.

Place Figure 2 here

The vehicle frames in the PyChrono module are defined using ISO 8855:2011. Fig. 3

presents an overview flowchart of the interactions of different modules during the simulation. As shown in Fig. 3, all subsystems can be customized in the simulation. For example, the vehicle type, the powertrain, and tires can be switched for different predefined vehicle types in the module, and the driver and terrain can be defined by assigning different values.

In this paper, the SCMDeformableTerrain module is used for the terrain to better represent the interaction between tire and soil. The model is defined by Gallina et al. [37] and its input parameters are summarized in Table. 1.

Place Figure 3 here

Place Table 1 here

Fig. 4 presents an example of the inputs and output of the off-road vehicle mobility prediction model. As indicated in the figure, the model takes a height map, soil parameters, and the coordinates of the path as input. Based on these inputs, it predicts the performance of a specific vehicle following a path in a defined area. Various vehicle characteristics including vehicle acceleration, vehicle speed along the path, and displacement of four wheels, can be simulated.

Place Figure 4 here

In general, for a given vehicle design Λ such as vehicle type, powertrain, tires, etc. as shown in Fig. 3, the mobility model of an off-road AGV can be represented as

Journal of Mechanical Design. Received August 19, 2021;
Accepted manuscript posted November 30, 2021. doi:10.1115/1.4053217

$$V(\mathbf{d}) = G(\mathbf{X}(\Lambda), \mathbf{Y}(\mathbf{d}), \Lambda), \tag{1}$$

where $\mathbf{d}$ are the spatial coordinates, $V(\mathbf{d})$ is the vehicle mobility at spatial location $\mathbf{d}$, $G(\cdot)$ is the mobility simulation model, $\mathbf{X}(\Lambda)$ are the vehicle-related parameters, such as vehicle weight, size, and power, and $\mathbf{Y}$ a function of spatial coordinate $\mathbf{d}$ representing the terrain-related parameters, such as slope, friction coefficient, cohesive limit, etc.

2.2 Deterministic Mission Planning

In deterministic mission planning, there are two types of subjects in a map $\mathbf{M}$: the free space $\mathbf{F}$, and the obstacle space $\mathbf{O}$, so that $\mathbf{M} = \mathbf{F} \cup \mathbf{O}$. The objective of mission planning is to generate an optimal path Ω_{opt} with the shortest distance while not crossing any obstacles as

$$\Omega_{opt} = \arg\min_{\Omega \in \mathbf{\Omega}} \ l(\Omega), \ \ \mathbf{d} \notin \mathbf{O} \ \forall \mathbf{d} \in \Omega, \tag{2}$$

where Ω is a feasible path in the candidate path set $\mathbf{\Omega}$, $l(\Omega)$ is the length of Ω, and $\mathbf{d}$ represents the coordinates of the path.

If there are no hard obstacles, such as big rocks or ravines, the off-road mobility model can provide a GO/NO-GO map based on the mean value of the terrain properties. The GO and NO-GO areas are respectively the free space and obstacle space as represented as:

$$\mathbf{F} = \left\{ \mathbf{d} \in \mathbf{M} \,|\, G(\bar{\mathbf{X}}(\Lambda), \bar{\mathbf{Y}}(\mathbf{d}), \Lambda) \geq e \right\}, \tag{3}$$

$$\mathbf{O} = \left\{ \mathbf{d} \in \mathbf{M} \,|\, G(\bar{\mathbf{X}}(\Lambda), \bar{\mathbf{Y}}(\mathbf{d}), \Lambda) < e \right\}, \tag{4}$$

where $\bar{\mathbf{X}}(\Lambda)$ and $\bar{\mathbf{Y}}(\mathbf{d})$ are the mean values of vehicle-related parameters and terrain-related parameters respectively, and e is the threshold of speed to determine whether the vehicle is stuck or not stuck at a certain location.

2.3 Off-Road AGV Mobility Reliability

2.3.1 Uncertainty sources in vehicle mobility analysis

As shown in Fig. 5, the uncertainty in the vehicle mobility analysis using Eq. (1) stems from two major sources, namely (1) uncertainty in vehicle modeling and simulation (M&S) and (2) uncertainty in the terrain-related parameters. The uncertainty sources in M&S usually remain constant over a target map, whereas the uncertainty of terrain-related parameters varies with the slope/soil type over space.

Place Figure 5 here

Furthermore, the uncertainty sources in M&S and soil maps can be classified into aleatory and epistemic uncertainty. Aleatory uncertainty represents the natural variability such as natural variability of vehicle physical parameters across a population of vehicles, variability of soil properties at different locations, etc. Epistemic uncertainty refers to the uncertainty due to lack of knowledge which is reducible if more information is available. Some representative examples of epistemic uncertainty in off-road AGV mobility analysis include model form uncertainty of the mobility prediction model, solution approximations, and data uncertainty in soil properties due to limited data.

Due to the heterogenous uncertainty sources in the M&S and soil properties, the vehicle mobility at each location is uncertain (see Fig. 5). The uncertainty of vehicle mobility can be quantified by propagating various uncertainty sources in both M&S and soil maps through a vehicle mobility simulation model. To propagate the uncertainty, various uncertainty sources must be modeled, which is not a trivial task since it requires a large volume of data from both vehicle systems and various soil samples. Some related data of the soil properties are available

in [37]. Vehicle-related uncertainty sources, however, vary with vehicle types and manufactures. In this paper, for the sake of illustration, vehicle-related uncertainty sources are not considered, since it is known that the variability of vehicle parameters are vehicle-dependent and are negligible compared to soil-related parameters[16]. Thus, we mainly focus on the uncertain terrain slope and soil properties as listed in Table 1. The developed framework, however, can be easily extended to incorporate other uncertainty sources if their statistical information is available.

As shown in Fig. 6, the soil type varies at different locations. For example, it may be sand (e.g., soil ID=l) at a location, or grass (e.g., soil ID=n) at a different location. Accordingly, the distributions of soil properties (e.g., friction or cohesive strength) are different for a sandy area or a grassland, for example. Moreover, there are several different soil properties for each soil type resulting in several different maps of soil parameters (see Fig. 6).

For any given spatial location $\mathbf{d}$ (Fig. 6), the slope/soil type is first identified and the statistical distribution of the uncertain soil/slope properties is determined. For example, the cumulative distribution function (CDF) of a soil parameter $Y_1(\mathbf{d})$ at location $\mathbf{d}$ can be represented as

$$\Pr\{Y_1(\mathbf{d}) \le y\} = \int_{-\infty}^{y} f_{Y_1}(y, \boldsymbol{\theta}(\mathbf{d}))dy, \tag{5}$$

in which $f_{Y_1}(y, \boldsymbol{\theta}(\mathbf{d}))$ is the probability density function (PDF) in terms of the distribution parameters $\boldsymbol{\theta}(\mathbf{d})$ which are statistical parameters determined by the slope/soil type at spatial location $\mathbf{d}$.

Place Figure 6 here

As mentioned previously, the distribution parameters $\boldsymbol{\theta}(\mathbf{d})$ can also be uncertain due to data uncertainty caused by limited geographic information system (GIS) data. In this paper, it is assumed that the distribution parameters $\boldsymbol{\theta}(\mathbf{d})$ are known, as shown in the numerical example section. We concentrate on how to identify a reliable path for a given soil property statistical distributions.

2.3.2 Vehicle mobility reliability

To quantitatively quantify the impact of various uncertainty sources on vehicle mobility, Jiang et. al. [5] defined two types of vehicle mobility reliability, namely vehicle state mobility reliability (SMR) and vehicle mission reliability (MMR).

SMR is defined as the probability that the maximum attainable speed $V(\mathbf{d})$ of an AGV at a certain location is greater than or equal to a predefined threshold e. It quantifies the probability that an AGV will not get stuck in a deformable soil or equivalently, the probability that a vehicle can remain mobile at a specific location. Mathematically, SMR at any location $\mathbf{d}$ or a given vehicle design Λ is given by

$$\begin{aligned} SMR(\mathbf{d}) &= \Pr\left\{V(\mathbf{d}) = G(\mathbf{X}(\Lambda), \mathbf{Y}(\mathbf{d}), \Lambda) \geq e\right\}, \\ &= \iint\limits_{G(\mathbf{X}(\Lambda), \mathbf{Y}(\mathbf{d}), \Lambda) \geq e} f_{\mathbf{X}}(\mathbf{x})\, f_{\mathbf{Y}}(\mathbf{y}, \boldsymbol{\theta}(\mathbf{d}))\mathbf{dxdy}, \end{aligned} \tag{6}$$

where $\Pr\{\cdot\}$ denotes probability, $f_{\mathbf{X}}(\mathbf{x})$ is the joint PDF of $\mathbf{X}(\Lambda)$, and e is a threshold of vehicle mobility.

MMR quantifies the probability of completing a mission considering the spatial dependence of various uncertainty sources on a given mission path Ω [5]. For a given Ω, MMR is defined as

$$MMR(\Omega) = \Pr\left\{V(\mathbf{d}) = G(\mathbf{X}(\Lambda), \mathbf{Y}(\mathbf{d}), \Lambda) \geq e, \forall \mathbf{d} \in \Omega\right\}, \tag{7}$$

in which $\forall$ means "for all".

Journal of Mechanical Design. Received August 19, 2021;
Accepted manuscript posted November 30, 2021. doi:10.1115/1.4053217

SMR and MMR quantify the mobility of a given vehicle design from different perspectives. The evaluation of these two types of reliability metrics is also different. Even though MMR is able to more comprehensively reflect the capability of an AGV than SMR from a mission perspective, the high computational complexity brings challenges to both mission planning and practical applications. In this paper, a bio-inspired approach is developed based on SMR to guarantee the reliability of AGVs on a path. The integration of the proposed method with MMR is even more complicated and will be investigated in future work.

The evaluation of the SMR in Eq. (6) is computationally challenging because of the high-dimensional integration. If the brute-force Monte Carlo simulation (MCS) is employed to estimate SMR, we can first generate N_{mcs} random realizations of soil parameters according to their spatial coordinates and statistical distributions. Based on that, the uncertainty of a soil property over a target map can be obtained by assembling together the random realizations at different locations. By propagating the N_{mcs} random realizations of soil properties through the vehicle mobility model, we obtain N_{mcs} realizations of $V(\mathbf{d})$ as $V^{(i)}(d),\ i=1,2,\cdots,N_{mcs}$. Based on that, the SMR at $\mathbf{d}$ can be approximated as

$$SMR(\mathbf{d}) \approx \frac{1}{N_{mcs}} \sum_{i=1}^{N_{mcs}} I(V_{\text{re}}^{i}(\mathbf{d}) \geq e), \quad \begin{cases} I=0, \text{ if } V_i < e \\ I=1, \text{ if } V_i \geq e \end{cases}. \tag{8}$$

The MCS-based method, however, is computationally prohibitive. In the next section, we first discuss how to overcome the computational challenge in vehicle mobility reliability analysis using an adaptive surrogate modeling method. Subsequently, we identify an optimal path based on the SMR analysis using a novel Physarum method.

3 Reliability-Based Mission Planning Using a Bio-Inspired Method

In order to incorporate post-design operation into design and guarantee the reliability of

AGV during operation in early design stages, the following reliability-based design optimization model must be solved

$$\begin{aligned} &\min\ C(\Lambda, \Omega), \\ &s.t. \\ &R(\Lambda, \Omega) \geq [R], \end{aligned} \tag{9}$$

where $C(\Lambda, \Omega)$ is a cost function of vehicle design Λ and path Ω controlling the post-design operation, $R(\Lambda, \Omega)$ is the vehicle mobility reliability, and $[R]$ is a mobility reliability requirement. The value of $[R]$ is determined by the decision maker according to the risk level he/she can accept. It is usually related to the economic loss of a vehicle failure event. For example, a high reliability is usually required if the consequence of failure is catastrophic.

In this paper, we fix the vehicle design and employ SMR as the mobility reliability constraint as discussed above. We will also include Λ in the design variables in future research. For given Λ, Eq. (9) reduces to the following optimization model

$$\begin{aligned} &\min_{\Omega}\ C(\Lambda, \Omega), \\ &s.t. \\ &\Pr\left\{V(\mathbf{d}) = G(\mathbf{X}(\Lambda), \mathbf{Y}(\mathbf{d}), \Lambda) \geq e\right\} \geq [R],\ \forall \mathbf{d} \in \Omega. \end{aligned} \tag{10}$$

Solving the above optimization model requires tackling two major challenges: (1) how to efficiently evaluate the probabilistic SMR constraint; and (2) how to solve the optimization model to identify the optimal path. In this paper, the first challenge is solved using an adaptive surrogate modeling method (Sec. 3.1) and the second challenge is addressed using a bio-inspired approach (Sec. 3.2).

3.1 Adaptive Surrogate Modeling for Model-Based Mobility Reliability Analysis

Evaluating the mobility reliability requires a large number of high-fidelity computer simulations, which is computationally very expensive. In order to reduce the required

computational cost in reliability analysis, various adaptive surrogate modeling methods have been developed in recent years to build an efficient yet accurate surrogate model of the original simulation model [38, 39]. The basic idea is to adaptively add new training data for surrogate modeling to improve the prediction accuracy in regions which are critical for reliability analysis. It has shown promising accuracy and efficiency for reliability analysis in various applications [40, 41]. For model-based mobility reliability analysis, our goal is to build a surrogate model of $V(\mathbf{d}) = G(\mathbf{X}(\Lambda), \mathbf{Y}(\mathbf{d}), \Lambda)$ to replace the original model.

We start with a Latin Hypercube sampling (LHS) of soil properties based on the low and upper bounds provided in [37] (Table 2). For each LHS sample, we use PyChrono to create a simulation model to predict the maximum attainable vehicle speed. As shown in Fig. 7, a terrain geometry is first created based on a terrain slope. The terrain is created long enough such that the vehicle can reach the maximum attainable speed. The deformable soil parameters are the values of a specific LHS sample. The vehicle is then commanded to accelerate from rest until the maximum steady vehicle speed is reached. Based on that, we obtained the maximum attainable speed for specific terrain slope and values of soil properties.

Place Table 2 here

Place Figure 7 here

Based on a number of initial samples, we can build a surrogate model $V(\mathbf{d}) = \hat{G}(\mathbf{X}, \mathbf{Y}(\mathbf{d}))$ using a Gaussian process (GP) surrogate modeling method to replace the original PyChrono simulation model. Note that since the vehicle design Λ is fixed in this paper, Λ is omitted

in the surrogate modeling for the sake of explanation. For any new sample $\mathbf{X}=\mathbf{x}$ and $\mathbf{Y(d)}=\mathbf{y}$, we predict the maximum attainable speed using the GP model as

$$V=\hat{G}(\mathbf{x},\mathbf{y})\sim N(\mu(\mathbf{z}),\sigma^2(\mathbf{z})), \tag{11}$$

where $\mathbf{z}\triangleq[\mathbf{x},\mathbf{y}]$, $N(\mu(\mathbf{z}),\sigma^2(\mathbf{z}))$ stands for normal distribution with a mean value of $\mu(\mathbf{z})$ and a standard deviation of $\sigma(\mathbf{z})$.

Since the initial surrogate model $V(\mathbf{d})=\hat{G}(\mathbf{X},\mathbf{Y}(\mathbf{d}))$ may not accurately represent the original simulation model, an adaptive Kriging Monte Carlo simulation (AK-MCS) method is then employed to improve the surrogate prediction accuracy in mobility reliability analysis [25, 42, 43]. Fig. 8 shows the flowchart of the adaptive surrogate modeling method. A large number of MCS samples are first generated for the variables given in Table 2. If the generated samples are $\mathbf{z}^{(i)}, i=1,2,\cdots,N_{mcs}$, we compute the U value of every sample using the following U learning function

$$U(\mathbf{z}^{(i)})=\left|\frac{\hat{L}(\mathbf{z}^{(i)})}{\sigma(\mathbf{z}^{(i)})}\right|=\left|\frac{\mu(\mathbf{z}^{(i)})-e}{\sigma(\mathbf{z}^{(i)})}\right|,\ \forall i=1,2,\cdots,N_{mcs}, \tag{12}$$

where $\mu(\mathbf{z}^{(i)})$ and $\sigma(\mathbf{z}^{(i)})$ are respectively the mean and standard deviation of the GP prediction (see Eq. (11)).

Place Figure 8 here

Based on the U values from Eq. (12), a new training sample $\mathbf{z}^{(i)}$ is identified as

$$i^*=\arg\min_i\{U(\mathbf{z}^{(i)})\}. \tag{13}$$

The identified new training sample is then added to the training data pool and the GP surrogate model is retrained using the updated training dataset. The process continues until the

smallest U value is greater than a certain threshold.

After we have an accurate surrogate model of the off-road AGV mobility, the surrogate model is used to predict the SMR according to the slope type and soil type at each location using Eq. (8). Since the SMR constraint of Eq. (10) requires that $SMR(\mathbf{d})$ at each location of a path Ω should be greater than $[R]$, we can rewrite the constraint given in Eq. (10) as follows

$$\begin{aligned} &\Pr\left\{V(\mathbf{d}) = G(\mathbf{X}(\Lambda), \mathbf{Y}(\mathbf{d}), \Lambda) \geq e\right\} \geq [R], \ \forall \mathbf{d} \in \Omega. \\ &\triangleq \Omega \in \boldsymbol{\Gamma}, \text{ where } \boldsymbol{\Gamma} = \{\forall \mathbf{d} \mid \Pr\left\{V(\mathbf{d}) = G(\mathbf{X}(\Lambda), \mathbf{Y}(\mathbf{d}), \Lambda) \geq e\right\} \geq [R]\}, \end{aligned} \tag{14}$$

in which $\boldsymbol{\Gamma}$ represents a set of coordinates $\mathbf{d}$ where $SMR(\mathbf{d}) \geq [R]$ is satisfied.

The above equation indicates that the optimization model of Eq. (10) can be solved in two sequential steps. In the *first* step, the coordinates $\mathbf{d}$ where the SMR constraint is satisfied are identified. To be consistent with the deterministic path planning, all the coordinates over a map $\mathbf{M}$ are classified into GO/NO-GO according to Eq. (14) as

$$\mathbf{d}_{GO} = \left\{\mathbf{d} \in \mathbf{M} \mid SMR(\mathbf{d}) \geq [R]\right\}, \tag{15}$$

$$\mathbf{d}_{NO-GO} = \left\{\mathbf{d} \in \mathbf{M} \mid SMR(\mathbf{d}) < [R]\right\}. \tag{16}$$

Based on the classification of the GO/NO-GO using the SMR constraint, Eq. (10) is written as a new model in the *second* step as

$$\begin{aligned} &\min_{\Omega} C(\Lambda, \Omega), \\ &s.t. \ \ \Omega \in \mathbf{d}_{GO}. \end{aligned} \tag{17}$$

In this paper, a bio-inspired approach is introduced to solve Eq. (17). It allows us to identify a path that satisfies the SMR constraint using model-based approach. Fig. 9 presents the flowchart of reliability-based mission planning. It starts with generating a mobility reliability map by identifying the soil/slope ID of each coordinate in the map. For a certain ID, random realizations of the slope and soil parameters are generated according to their statistical

distributions. Using the trained mobility surrogate model, random realizations of vehicle mobility are obtained for each coordinate of the target map. Based on the random realizations, a SMR map is generated, and subsequently a GO/NO-GO map is obtained using Eqs. (15) and (16).

Place Figure 9 here

Treating the NO-GO coordinates as obstacles, the next question is how to efficiently solve Eq. (17) to identify an optimal path for an off-road AGV to go from a starting point to a target point (see Fig. 9(e)-(f)). It is worth mentioning that the "obstacles" considered here are different from the conventional "hard" obstacles in path planning of robotics. In common seen robotics path planning problems, the "hard" obstacles are detected using cameras or lidars if the robots are close to the obstacles. Because the obstacles are detectable, paths of robots can be re-planned. In such a case, a globally optimal and reliable path may not be very important. For the off-road AGV, however, the obstacles are not real/hard. Instead, they represent the probability that a vehicle may get stuck at the obstacle location. They cannot be directly detected by a camera or a lidar. Taking a mud pond as an example, a vehicle can sometimes pass the mud pond and sometimes get stuck in it. Even if a camera can detect the existence of a mud pond, it cannot tell if a vehicle can pass it or get stuck in it. It would be too late if we wait for the vehicle to get stuck in the mud pond and then perform the re-planning. This is the reason a globally optimal and reliable path is particularly important for an off-road AGV.

For reliable path planning of off-road AGVs, approaches have been developed using RRT* [5]. Another widely used approach is the Dijkstra-based method [44]. Even though these approaches have shown promising performance in identifying an optimal path, we noticed that

the required computational time is still high especially for multi-vehicle path planning problems where the algorithms must be run multiple times. In this paper, we suggest an alternative path planning algorithm to solve the optimization model of Eq. (17) for off-road AGVs using a bio-inspired Physarum method [45]. To the best of our knowledge, this is the first time a bio-inspired approach is employed for path planning of off-road AGVs. As shown in the numerical example section, the Physarum approach shows better performance than the Dijkstra-based method. Section 3.2 provides more details of the Physarum-based mission planning method.

3.2 Physarum solver-based mission planning

In order to integrate the Physarum method with the GO/NO-GO map generated from the mobility reliability analysis of Sec. 3.1 (i.e. solve Eq. 17) and to further reduce the computational effort in mission planning, we first need to convert the GO/NO-GO map corresponding to any mobility reliability requirement into a network described by nodes and edges. To accomplish such a conversion, the following navigation mesh method is employed.

3.2.1 Navigation mesh

There are many ways to convert the GO/NO-GO map into a network. A straightforward way of doing that is to connect every non-obstacle coordinate with all its non-obstacle neighborhood coordinates. This method is usually referred to as *uniform mesh* (Fig. 10(b)). The uniform mesh allows to cover all locations in a map and thus achieves high accuracy in path planning. However, the number of nodes and edges increases exponentially with the size of the target map, which significantly increases the required computational cost of path planning and hinders the practical application of the uniform mesh in off-road AGV mission planning. This disadvantage of uniform mesh exists for both the commonly used Dijkstra algorithm and the

physarum algorithm presented in Sec. 3.2.2.

As an alternative, the navigation mesh is widely used for path finding in game design [46, 47]. It partitions a map into polygons, and a network is built by connecting the center or the vertex of the polygons. Fig. 10 compares the uniform and navigation meshes for a GO/NO-GO map given in Fig. 10(a).

Place Figure 10 here

As shown in Fig. 10, the navigation mesh drastically reduces the number of nodes and edges of the resulting network. Therefore, it can significantly reduce the computational time in mission planning. The disadvantage of navigation mesh, however, is that it sacrifices accuracy. The identified paths may not be the truly globally optimal, since the path depends on the defined edges and nodes. However, this disadvantage can be overcome by tuning the relevant parameters in generating the mesh. In this paper, a Python package named Triangle [48] is employed to convert a GO/NO-GO map into a network for mission planning. It is built based on Jonathan Richard Shewchuk's two-dimensional quality mesh generator and Delaunay triangulator library [49]. The employment of a navigation mesh in conjunction with the adaptive surrogate modeling method drastically reduces the required computational effort of mission planning from different perspectives.

Next, we discuss how to identify optimal paths for a single vehicle and multi-vehicle scenarios by using a bio-inspired physarum solver and the navigation mesh.

3.2.2 Physarum solver

Physarum polycephalum is a bio-inspired path planner originally proposed by Nakagaki et al. [50], who demonstrated that Physarum could disassemble and reassemble the tube structure

and tube thickness over time in response to the change of external conditions (availability of food sources) to identify the shortest path connecting the food sources. As shown in Fig. 11, this organism can form a tube forming the shortest path connecting two food sources located at the source point (s) and the sink point (t) in the maze. The mathematical model of the path generator in the network-based map was proposed by Tero et al. [45].

Place Figure 11 here

Suppose we represent the maze with a graph G, in which two nodes s and t are designated as the starting and ending nodes. The other nodes are labelled as $n_1, n_2, \cdots, n_i$ etc. The edge between nodes n_i and n_j is represented by e_{ij}. The set of all edges is denoted by E. For a network-based map as shown in Fig. 11, the flux Q_{ij} through edge e_{ij} is formulated following the Poiseuille flow assumption as

$$Q_{ij} = \frac{D_{ij}}{L_{ij}}(p_i - p_j), \tag{18}$$

where p_i is the pressure at node n_i, L_{ij} is the length of edge e_{ij}, and D_{ij} is its conductivity.

Since the inflow and outflow should be balanced, Kirchhoff's law yields:

$$\begin{cases} \sum_i Q_{ij} + I_0 = 0, & j = s, \\ \sum_i Q_{ij} - I_0 = 0, & j = t, \\ \sum_{\forall (i,j) \in E} Q_{ij} = 0, & \text{otherwise} \end{cases}, \tag{19}$$

where I_0 is the flux from the source node.

Journal of Mechanical Design. Received August 19, 2021;
Accepted manuscript posted November 30, 2021. doi:10.1115/1.4053217

To simplify the problem, we let $I_0 = 1$ [51]. By combining Eqs. (18) and (19), we have [45]:

$$\sum_i \frac{D_{ij}}{L_{ij}}(p_i - p_j) = \begin{cases} -1, & j = s, \\ 1, & j = t, \\ 0, & \text{otherwise} \end{cases}, \tag{20}$$

where all p_i can be determined by solving the linear system of equations (20). Afterwards, the flux through each edge e_{ij} is derived using Eq. (18) accordingly.

In order to formulate the conductivity change for each edge, we have

$$\frac{dD_{ij}}{dt} = f(|Q_{ij}|) - rD_{ij}, \tag{21}$$

where $f(x)$ is an increasing function satisfying $f(0) = 0$.

To save computational effort, we let $f(x) = x$ and $r = 1$, so that

$$\frac{D_{ij}^{m+1} - D_{ij}^{m}}{\delta t} = |Q_{ij}^{m}| - D_{ij}^{m+1}, \tag{22}$$

where m represents the m^{th} iteration and $\delta t = 1$. Based on the above equations, an optimal path can be identified for any given map [45].

After generating the navigation mesh, Fig. 12 shows the flowchart of the Physarum-based path planning approach. In the figure, th is the threshold to determine whether the conductivity matrix $\mathbf{D}$ has converged.

Place Figure 12 here

In order to calculate the pressure at each node, we must solve Eq. (20). The matrix expression of Eq. (20) is

$$\mathbf{A} \cdot \mathbf{p} = \mathbf{C}, \tag{23}$$

Journal of Mechanical Design. Received August 19, 2021;
Accepted manuscript posted November 30, 2021. doi:10.1115/1.4053217

where $\mathbf{A} \in \mathbb{R}_{n\times n}$ is given by

$$\mathbf{A} = \frac{\mathbf{D}}{\mathbf{L}} = \begin{bmatrix} A_{11} & A_{12} & \cdots & A_{1n} \\ A_{21} & A_{22} & \cdots & A_{2n} \\ \vdots & \vdots & \ddots & \vdots \\ A_{n1} & A_{n2} & \cdots & A_{nn} \end{bmatrix} = \begin{bmatrix} \frac{D_{11}}{L_{11}} & \cdots & \frac{D_{1n}}{L_{1n}} \\ \vdots & \ddots & \vdots \\ \frac{D_{n1}}{L_{n1}} & \cdots & \frac{D_{nn}}{L_{nn}} \end{bmatrix}, \quad A_{ii} = -\sum_j A_{ij}, \tag{24}$$

$\mathbf{D} \in \mathbb{R}_{n\times n}$ is the conductivity matrix, $\mathbf{L} \in \mathbb{R}_{n\times n}$ is the length matrix of the network, and $\mathbf{D}$, $\mathbf{L}$, and $\mathbf{p}$ are given by

$$\mathbf{D} = \begin{bmatrix} D_{11} & D_{12} & \cdots & D_{1n} \\ D_{21} & D_{22} & \cdots & D_{2n} \\ \vdots & \vdots & \ddots & \vdots \\ D_{n1} & D_{n2} & \cdots & D_{nn} \end{bmatrix}. \tag{25}$$

$$\mathbf{L} = \begin{bmatrix} L_{11} & L_{12} & \cdots & L_{1n} \\ L_{21} & L_{22} & \cdots & L_{2n} \\ \vdots & \vdots & \ddots & \vdots \\ L_{n1} & L_{n2} & \cdots & L_{nn} \end{bmatrix}, L_{ij} = +\infty \text{ when no connection between } i, j. \tag{26}$$

$$\mathbf{p} = [p_1, p_2, \cdots, p_n]^T, \tag{27}$$

and

$$\mathbf{C} = [C_1, C_2, \cdots, C_n]^T, \; C_i = -1 \text{ when } i = s, \; C_i = 1 \text{ when } i = t. \tag{28}$$

Once the conductivity matrix $\mathbf{D}$ reaches a steady state, an optimal path can be identified by selecting the edges with the largest conductivity that form a path connecting the starting point with the target point.

Algorithm 1 shows the general procedure of Physarum-based method, including the updating of the conductivity matrix and the identification of the optimal path after the conductivity matrix converges.

Journal of Mechanical Design. Received August 19, 2021;
Accepted manuscript posted November 30, 2021. doi:10.1115/1.4053217

Place Algorithm 1 here

This algorithm can also handle dynamic path planning problem. If there are new edges between nodes i and j, or new obstacles that cut the edges between node i and j, we simply need to change L_{ij} from infinity to l or from l to infinity. Using the previous conductivity matrix $\mathbf{D}$, the knowledge of the remaining part of the map that has not changed is carried into the new calculation saving computational time.

Moreover, the Physarum-based method can naturally accommodate the task of multi-vehicle mission planning including automatic vehicle assignments and identification of optimal path for each vehicle. The procedure is similar to single vehicle path planning. The difference is that there are more than one starting point and target point. As a result, $\mathbf{C}$ in Eq. (23) becomes

$$\mathbf{C}=[C_1,C_2,\cdots,C_n]^T,\ C_i=-1 \text{ when } i\in\mathbf{s},\ C_i=1 \text{ when } i\in\mathbf{t}, \tag{29}$$

where $\mathbf{s}$ and $\mathbf{t}$ are the group of starting points and target points.

After the conductivity matrix converges, we can identify an optimal path by starting with any starting point and using the path identification part in Algorithm 1. For the remaining starting points, we must update the conductivity matrix based on the edges selected by the last path as

$$D_{ij}^{*}=\begin{cases} D_{ij}-1, & \text{if } D_{ij}>1 \\ 0.8D_{ij}, & \text{otherwise} \end{cases}, \forall ij \text{ satisfies } e_{ij}\in\Omega_{last}, \tag{30}$$

where D_{ij}^{*} represents the updated conductivity value of edge e_{ij}, and Ω_{last} is the last optimal path found by Algorithm 1. Noted that it includes multiple edges.

Finally, we repeat the procedure in Algorithm 1 using the updated conductivity matrix to

identify another optimal path, until every starting point is assigned to a target point.

3.3 Implementation Procedure

Fig. 13 summarizes the overall implementation procedure of the proposed reliability-based mission planning framework. It includes off-road vehicle mobility modeling, reliability-based map generation, network-based meshing, and Physarum-based path planning.

Place Figure 13 here

In the Section 4, we use a case study to demonstrate the efficacy of the proposed method for path planning under uncertainty.

4 Numerical Example

In this numerical example, we first construct a surrogate model of the off-road mobility model using the approach of Section 3. Then, we convert a soil and slope map of interest into a mobility reliability map and the GO/NO-GO map. After that, two case studies are used to demonstrate the effectiveness of the proposed Physarum solver-based approach in conjunction with a navigation mesh for both a single vehicle and multi-vehicle mission planning in off-road environments.

4.1 Maps of Interest

Fig. 14 presents the slope map and a soil map of interest for mission planning. These maps are created manually to demonstrate the proposed framework. They are discretized using 60 points in both coordinate d_1 and d_2. Also, there are 6 different slope intervals and soil types

represented by different slope and soil IDs. Each slope ID represents a slope parameter and each soil ID represents 6 soil parameters in the PyChrono simulation model, including Bekker_Kphi (k_ϕ), Bekker_Kc (k_c), Bekker_n (B_n), Mohr_cohesion (c), Mohr_friction (ϕ), and Janosi_shear (J). In this paper, all parameters are assumed to follow the Gaussian distribution for the sake of illustration. The proposed framework is applicable to any type of statistical distributions. Table 3 shows the statistical information of the parameters corresponding to different slope/soil IDs.

Place Figure 14 here

Place Table 3 here

4.2 Generation of Mobility Reliability Map

In order to predict the vehicle mobility under different off-road environment considering various uncertainty sources, we first construct a surrogate model for the mobility prediction using the adaptive surrogate modeling method presented in Section 3.1. In the PyChrono simulation, the HMMWV vehicle system is used including the vehicle body, powertrain and tires as shown in Fig. 15. The vehicle uses full double wishbone suspensions and a Pitman arm steering mechanism [29].

Place Figure 15 here

Journal of Mechanical Design. Received August 19, 2021;
Accepted manuscript posted November 30, 2021. doi:10.1115/1.4053217

In the adaptive surrogate modeling, we first generated 100 training points as the initial training points. A radial basis function kernel plus a white noise kernel is used in the Gaussian process modeling. The surrogate model is then adaptively refined in critical regions using the learning function given in Eq. (9) with parameter $e = 2m/s$. Fig. 16(a) presents the convergence history of the U values in the adaptive training. As shown, $U_{\min}$ reached the threshold $U_{th} = 2$ after 60 iterations. To verify the effectiveness of the adaptive surrogate modeling method, we compare its prediction accuracy of mobility reliability for a certain soil type with its counterparts obtained from: (1) a global surrogate modeling with 1300 training points and (2) surrogate modeling by adaptively minimizing the variance. Fig. 16(b) shows that the adaptive surrogate modeling using the learning function given in Eq. (9) is more accurate and converges faster than the commonly used variance minimization approach. This demonstrates the efficacy of adaptive surrogate modeling in efficiently constructing a mobility surrogate model for vehicle mobility reliability analysis.

After the surrogate model is properly trained, it was used to predict vehicle mobility for different slopes and soil parameters. For the maps in Fig. 14, $N_{MCS} = 10000$ Monte Carlo samples are generated for each slope/soil parameters according to their statistical distributions. Based on the samples and the mobility surrogate model, a probabilistic mobility map and a mobility reliability map was obtained. Fig. 17(a) shows the mobility map obtained using the mean values of the soil properties. Fig. 17(b) shows the state mobility reliability (SMR) map obtained using Eq. (7).

Place Figure 16 here

Place Figure 17 here

With the SMR map, the GO/NO-GO map can be easily generated using Eqs. (11) and (12). Fig. 18 shows three different maps for different value of R_t.

Place Figure 18 here

As Fig.18 shows, changing the reliability threshold could lead to different GO/NO-GO maps. The number of obstacles increases with reliability level. An increased reliability level will lead to an increased length of the shortest path. This implies that the vehicle must sacrifice travel time to ensure mobility reliability. The decision maker needs to determine an optimal reliability requirement by considering the consequence of failure to achieve a tradeoff between travel time and mobility reliability. By setting $R_t = 0.9$, we then converted the corresponding GO/NO-GO map into the navigation mesh (Fig. 19). Now the map is ready to be used for mission planning subject to the constraint that SMR should be greater than 0.9. Thus, the paths identified based on the map satisfy the mobility reliability requirement of at least 0.9. Next, we investigate two case studies, namely a single vehicle and multi-vehicles, using the obtained navigation mesh.

4.3 Case Study 1: Path Planning for a Single Vehicle

Fig. 20 (a) shows the starting point (S) and target point (T) for this case study. The Physarum solver-based approach must find the shortest path between S and T. As Fig. 20 (b) shows, while the vehicle follows the shortest path and reaches the middle of the path (M), a new obstacle appears in the map. The vehicle must dynamically update the path based on the

new map starting from the current point M. Also, it needs to update the shortest path between the initial starting point S and target point T for future vehicles.

Place Figure 19 here

Place Figure 20 here

Fig. 21 presents the identified optimal paths that satisfy the reliability requirement. The paths include (a) a shortest path connecting the starting and target points, (b) an optimal path for the situation of dynamic path planning, and (c) an optimal path if new obstacle appears on the map for future vehicles.

Place Figure 21 here

Table 4 compares the proposed Physarum algorithm and the widely used Dijkstra approach for this first case study which identifies a path connecting the starting and target points. The results show that even though both approaches are able to identify the optimal paths for different scenarios, the Dijkstra-based approach is faster than the Physarum algorithm for a single vehicle path planning under uncertainty.

Place Table 4 here

4.4 Case Study 2: Mission Assignment and Planning for Multiple Vehicles

As shown in Fig. 22, in this case, there are three starting points and three target points. The decision maker must find the best combination between starting and target points in order to minimize the overall length. A dynamic obstacle also appears in the map as shown in Fig. 22(b). The approach must re-plan the path from the starting point if a new obstacle appears and still minimize the overall length.

Place Figure 22 here

The Physarum algorithm only needs to generate three different paths for each starting point, while the Dijkstra algorithm must generate all nine possible pairs. Fig. 23 presents the results of the Physarum algorithm for the original path planning and the dynamic path planning. Table 5 compares the Physarum and Dijkstra algorithms. Based on the results in the table, we observe that the proposed Physarum algorithm reduces the computational time by directly providing the optimal solution. It outperforms the Dijkstra algorithm for the problem of multi-vehicle assignment under uncertainty.

Place Figure 23 here

Place Table 5 here

Journal of Mechanical Design. Received August 19, 2021;
Accepted manuscript posted November 30, 2021. doi:10.1115/1.4053217

5 CONCLUSIONS

This paper proposes a Physarum algorithm for model-based path planning under uncertainty subject to a mobility reliability constraint. A simulation model is first used to generate the training data to build a surrogate model for the vehicle mobility. An adaptive surrogate modeling approach is employed to further improve the accuracy of the surrogate model. Using the vehicle mobility surrogate model, a GO/NO-GO map is generated by specifying a vehicle state mobility reliability requirement. Finally, a Physarum algorithm is combined with a navigation mesh to perform mission planning of single and multiple vehicles in a dynamic environment with a specific reliability requirement. According to the results of the two case studies, the proposed method is capable of finding the shortest path in a network-based map. Although the Physarum algorithm is slower than the Dijkstra algorithm for a single vehicle path planning, it is faster than Dijkstra for multi-vehicle path planning problems. Moreover, the results show that if the number of vehicles increases from 1 to 3, the planning time of the Dijkstra algorithm increases from 0.14s to 1.06s (around 8 times) while that of Physarum algorithm changes only from 0.66s to 0.69s (basically the same). The proposed method can also handle dynamic path planning problems very well.

The Physarum solver uses a GO/NO-GO map as input to identify the shortest paths satisfying specific mobility reliability constraints. The GO/NO-GO map is obtained by considering various uncertainty sources in model-based simulations. As a result, the aleatoric and epistemic uncertainty sources will affect the results of shortest path indirectly. If the GO/NO-GO map is not generated correctly, the identified shortest path will subject to either high risk of mobility failure or being unnecessarily long. In this paper, we only considered the aleatoric uncertainty in generating the GO/NO-GO map. The impact of various epistemic uncertainty sources in reducing the shortest path is worth investigating in future work. In

addition, a reliability-based path/mission planning is performed in this paper for a given vehicle design. The concurrent design optimization of vehicle physical systems and the post-design path/mission planning could also be addressed in future work.

ACKNOWLEDGEMENT

This work was supported in part by the Automotive Research Center (ARC) in accordance with Cooperative Agreement W56HZV-04-2-0001 U.S. Army CCDC Ground Vehicle Systems Center (GVSC), Warren, MI. The support is gratefully acknowledged.

REFERENCES

[1] Liu, Q., Zhao, L., Tan, Z., and Chen, W., 2017, "Global path planning for autonomous vehicles in off-road environment via an A-star algorithm," International Journal of Vehicle Autonomous Systems, 13(4), pp. 330-339.

[2] Oksanen, T., and Visala, A., 2009, "Coverage path planning algorithms for agricultural field machines," Journal of field robotics, 26(8), pp. 651-668.

[3] Coombs, D., Murphy, K., Lacaze, A., and Legowik, S., "Driving autonomously off-road up to 35 km/h," Proc. Proceedings of the IEEE Intelligent Vehicles Symposium 2000 (Cat. No. 00TH8511), IEEE, pp. 186-191.

[4] Quann, M., Ojeda, L., Smith, W., Rizzo, D., Castanier, M., and Barton, K., 2020, "Off-road ground robot path energy cost prediction through probabilistic spatial mapping," Journal of Field Robotics, 37(3), pp. 421-439.

[5] Jiang, C., Hu, Z., Mourelatos, Z. P., Gorsich, D., Jayakumar, P., Fu, Y., and Majcher, M., 2021, "R2-RRT*: Reliability-Based Robust Mission Planning of Off-Road Autonomous Ground Vehicle Under Uncertain Terrain Environment." IEEE Transactions on Automation Science and Engineering, DOI: 10.1109/TASE.2021.3050762.

[6] McCullough, M., Jayakumar, P., Dasch, J., and Gorsich, D., "The next generation NATO reference mobility model development," Journal of Terramechanics, 73, pp. 49-60.

[7] Petrick, E., Janosi, Z., and Haley, P., 1981, "The use of the nato reference mobility model in military vehicle procurement," No. 0148-7191, SAE Technical Paper.

[8] Bradbury, M., Dasch, J., Gonzalez, R., Hodges, H., Jain, A., Iagnemma, K., Letherwood, M., Mccullough, M., Priddy, J., And Wojtysiak, B., 2016, "Next-Generation NATO Reference Mobility Model (NG-NRMM)," Tank Automotive Research, Development and Engineering Center (TARDEC) Warren United States.

[9] McCullough, M., Jayakumar, P., Dasch, J., and Gorsich, D., 2016, "Developing the Next Generation NATO Reference Mobility Model," US ARMY TARDEC WARREN United States.

[10] Yamashita, H., Jayakumar, P., Alsaleh, M., and Sugiyama, H., 2018, "Physics-based deformable tire–soil interaction model for off-road mobility simulation and experimental validation," Journal of Computational and Nonlinear Dynamics, 13(2).

[11] Laughery, S., Gerhart, G., and Goetz, R., 1990, "Bekker's terramechanics model for off-road vehicle research," TACOM Research Development And Engineering Center Warren MI.

[12] Hetherington, J. G., 2001, "The applicability of the MMP concept in specifying off-road mobility for wheeled and tracked vehicles," Journal of terramechanics, 38(2), pp. 63-70.

[13] Gonzalez, R., Jayakumar, P., and Iagnemma, K., 2017, "Generation of stochastic mobility maps for large-scale route planning of ground vehicles: A case study," Journal of Terramechanics, 69, pp. 1-11.

[14] Haug, E. J., Adkins, F. A., and Coroian, D., 1998, "Domains of mobility for a planar body moving among obstacles," ASME-Journal of Mechanical Design, 120(3), pp. 462-467.

[15] González, R., Jayakumar, P., and Iagnemma, K., 2017, "Stochastic mobility prediction of ground vehicles over large spatial regions: a geostatistical approach," Autonomous Robots, 41(2), pp. 311-331.

[16] Choi, K., Jayakumar, P., Funk, M., Gaul, N., and Wasfy, T. M., 2019, "Framework of reliability-based stochastic mobility map for next generation nato reference mobility model," Journal of Computational and Nonlinear Dynamics, 14(2).

[17] J Jayakumar, P., and Mechergui, D., 2019, "Efficient generation of accurate mobility maps using machine learning algorithms," US ARMY TARDEC Warren United States.

[18] Hu, Z., Mourelatos, Z. P., Gorsich, D., Jayakumar, P., and Majcher, M., 2020, "Testing Design Optimization for Uncertainty Reduction in Generating Off-Road Mobility Map Using a Bayesian Approach," ASME-Journal of Mechanical Design, 142(2).

[19] Yang, D., 1993, "Collision-free path planning by using nonperiodic B-spline curves," ASME-Journal of Mechanical Design, 115(3), pp. 679-684.

[20] Melchior, N. A., and Simmons, R., "Particle RRT for path planning with uncertainty," Proc.

Proceedings 2007 IEEE International Conference on Robotics and Automation, IEEE, pp. 1617-1624.

[21] Sun, W., van den Berg, J., and Alterovitz, R., 2016, "Stochastic extended LQR for optimization-based motion planning under uncertainty," IEEE Transactions on Automation Science and Engineering, 13(2), pp. 437-447.

[22] Van Den Berg, J., Abbeel, P., and Goldberg, K., 2011, "LQG-MP: Optimized path planning for robots with motion uncertainty and imperfect state information," The International Journal of Robotics Research, 30(7), pp. 895-913.

[23] Zhang, B., Mao, Z., Liu, W., and Liu, J., 2015, "Geometric reinforcement learning for path planning of UAVs," Journal of Intelligent & Robotic Systems, 77(2), pp. 391-409.

[24] Chao, N., Liu, Y.-k., Xia, H., Ayodeji, A., and Bai, L., 2018, "Grid-based RRT∗ for minimum dose walking path-planning in complex radioactive environments," Annals of Nuclear Energy, 115, pp. 73-82.

[25] Liu, Y., Jiang, C., Mourelatos, Z. P., Gorsich, D., Jayakumar, P., Fu, Y., Majcher, M., and Hu, Z., 2021, "Simulation-Based Mission Mobility Reliability Analysis of Off-Road Ground Vehicles," ASME-Journal of Mechanical Design, 143(3).

[26] Sampedro, C., Bavle, H., Sanchez-Lopez, J. L., Fernández, R. A. S., Rodríguez-Ramos, A., Molina, M., and Campoy, P., 2016, "A flexible and dynamic mission planning architecture for uav swarm coordination," Proc. 2016 International Conference on Unmanned Aircraft Systems (ICUAS), IEEE, pp. 355-363.

[27] Wei, Y., Madey, G. R., and Blake, M. B., 2013, "Agent-based simulation for uav swarm mission planning and execution," Proc. Proceedings of the Agent-Directed Simulation Symposium, pp. 1-8.

[28] Dui, H., Zhang, C., Bai, G., and Chen, L., 2021, "Mission Reliability Modeling of UAV Swarm and Its Structure Optimization based on importance measure," Reliability Engineering & System Safety, p. 107879.

[29] "PYCHRONO: A Multi-physics Simulation Engine." , Project Chrono, last modified Feb 14 2021, https://projectchrono.org/pychrono/.

[30] Serban, R., Olsen, N., Negrut, D., Recuero, A., and Jayakumar, P., "A co-simulation framework for high-performance, high-fidelity simulation of ground vehicle-terrain interaction," Proc. Conference: NATO AVT-265 Specialists' Meeting, Vilnius, Lithuania (May 2017), p. 24.

[31] Rubinstein, D., and Hitron, R., 2004, "A detailed multi-body model for dynamic simulation of off-road tracked vehicles," Journal of Terramechanics, 41(2-3), pp. 163-173.

[32] Liang, C.-Y., Allen, R. W., Rosenthal, T. J., Chrstos, J. P., and Nunez, P., 2004, "Tire modeling for off-road vehicle simulation," SAE transactions, pp. 1063-1073.

[33] Krenn, R., and Gibbesch, A., 2011, "Soft soil contact modeling technique for multi-body system simulation," Trends in computational contact mechanics, pp. 135-155.

[34] Senatore, C., and Sandu, C., 2011, "Off-road tire modeling and the multi-pass effect for vehicle dynamics simulation," Journal of Terramechanics, 48(4), pp. 265-276.

[35] Tasora, A., Serban, R., Mazhar, H., Pazouki, A., Melanz, D., Fleischmann, J., Taylor, M., Sugiyama, H., and Negrut, D., 2015, "Chrono: An open source multi-physics dynamics engine," Proc. International Conference on High Performance Computing in Science and Engineering, Springer, Cham, May 25, 2015, pp. 19-49.

[36] Serban, R., Taylor, M., Negrut, D., and Tasora, A., 2019, "Chrono:: Vehicle: template-based ground vehicle modelling and simulation," International Journal of Vehicle Performance, 5(1), pp. 18-39.

[37] Gallina, A., Krenn, R., Scharringhausen, M., Uhl, T., and Schäfer, B., 2014, "Parameter identification of a planetary rover wheel–soil contact model via a Bayesian approach," Journal of Field Robotics, 31(1), pp. 161-175.

[38] Hu, Z., and Mahadevan, S., 2016, "Global sensitivity analysis-enhanced surrogate (GSAS) modeling for reliability analysis," Structural and Multidisciplinary Optimization, 53(3), pp. 501-521.

[39] Hu, Z., and Mahadevan, S., 2018, "Adaptive surrogate modeling for time-dependent multidisciplinary reliability analysis," ASME-Journal of Mechanical Design, 140(2).

[40] Kaminsky, A. L., Wang, Y., and Pant, K., 2021, "An Efficient Batch K-Fold Cross-Validation Voronoi Adaptive Sampling Technique for Global Surrogate Modeling," ASME-Journal of Mechanical Design, 143(1), p. 011706.

[41] Zhang, Y., Kim, N. H., and Haftka, R. T., 2020, "General-surrogate adaptive sampling using interquartile range for design space exploration," ASME-Journal of Mechanical Design, 142(5).

[42] Echard, B., Gayton, N., and Lemaire, M., 2011, "AK-MCS: an active learning reliability method combining Kriging and Monte Carlo simulation," Structural Safety, 33(2), pp. 145-154.

[43] Fauriat, W., and Gayton, N., 2014, "AK-SYS: an adaptation of the AK-MCS method for

system reliability," Reliability Engineering & System Safety, 123, pp. 137-144.

[44] Deng, Y., Chen, Y., Zhang, Y., and Mahadevan, S., 2012, "Fuzzy Dijkstra algorithm for shortest path problem under uncertain environment," Applied Soft Computing, 12(3), pp. 1231-1237.

[45] Tero, A., Kobayashi, R., and Nakagaki, T., 2006, "Physarum solver: A biologically inspired method of road-network navigation," Physica A: Statistical Mechanics and its Applications, 363(1), pp. 115-119.

[46] Hartley, T. P., and Mehdi, Q. H., "In-game adaptation of a navigation mesh cell path," Proc. 2012 17th International Conference on Computer Games (CGAMES), Jul 30, 2012, IEEE, pp. 230-236.

[47] Xu, X., Huang, M., and Zou, K., 2011, "Automatic generated navigation mesh algorithm on 3D game scene," Procedia Engineering, 15, pp. 3215-3219.

[48] "Triangle 20200404 documentation," https://rufat.be/triangle/#triangle.

[49] Shewchuk, J.R., 2008, "A two-dimensional quality mesh generator and Delaunay triangulator," Computer Science Division University of California at Berkeley, Berkeley, California, http://www. cs. cmu. edu/quake/triangle. html, pp.94720-1776.

[50] Nakagaki, T., Yamada, H., and Tóth, Á., 2000, "Maze-solving by an amoeboid organism," Nature, 407(6803), pp. 470-470.

[51] Zhang, X., Chan, F. T., Yang, H., and Deng, Y., 2017, "An adaptive amoeba algorithm for shortest path tree computation in dynamic graphs," Information Sciences, 405, pp. 123-140.

List of Table Captions

List of Figure Captions

Journal of Mechanical Design. Received August 19, 2021;
Accepted manuscript posted November 30, 2021. doi:10.1115/1.4053217

Table 1 Input parameters of the SCMDeformableTerrain module

Map parameter	Size parameter	Soil parameter
Height map	sizeX	Bekker_Kphi
	sizeY	Bekker_Kc
	hMin	Bekker_n
	hMax	Mohr_cohesion
		Mohr_friction
		Janosi_shear

Table 2 Input interval of parameters of the SCMDeformableTerrain module

Parameters		Lower Bound	Upper Bound
Slope-related	Slope	0	45°
Soil-related	Bekker_Kphi	1	10^9
	Bekker_Kc	1	10^{10}
	Bekker_n	0.8	2
	Mohr_cohesion	22.5°	37.5°
	Mohr_friction	0.001	0.05
	Janosi_shear	0	1000

Journal of Mechanical Design. Received August 19, 2021;
Accepted manuscript posted November 30, 2021. doi:10.1115/1.4053217

Algorithm 1: Physarum algorithm for single vehicle path planning

Data: **L** is the length matrix given in Eq. (26), *s* is the start point, *t* is the target point, and *n* is the size of the network

Initialization: $D_{ij}=0.5,\ Q_{ij}=0,\ p_i=0,\ \forall i, j=1,2,\cdots,n.$

While sum($|d\mathbf{D}|$)>*th* **do**

Calculate pressure using Eq. (20)

$$\sum_i \frac{D_{ij}}{L_{ij}}(p_i-p_j)=\begin{cases}-1, & j=s\\ 1, & j=t\\ 0 & otherwise\end{cases}$$

$Q_{ij}=\frac{D_{ij}}{L_{ij}}(p_i-p_j)$, // Using Eq. (18)

$D_{ij}=0.5\left(\left|Q_{ij}\right|+D_{ij}\right)$ // Using Eq. (21)

$d\mathbf{D}=\left|\mathbf{D}^{n+1}-\mathbf{D}^{n}\right|$ // Calculate the change of the conductivity

path=[], *ind=s, path.append(ind)*

While *ind*≠*t* **do**

$ind_{next}=\arg\max_i(\mathbf{D}_{ind,\cdot})$, where $\mathbf{D}_{ind,\cdot}=[D_{ind,1},D_{ind,2},\cdots,D_{ind,n}]$

path.append(ind_{next}*)*

$D_{ind_{next},\,path[-1]}=0$, where $path[-1]$ represents the last element of *path*, and $\mathbf{D}_{\cdot,ind}=0$, where $\mathbf{D}_{\cdot,ind}=[D_{1,ind},D_{2,ind},\cdots,D_{n,ind}]$

$ind=ind_{next}$

Journal of Mechanical Design. Received August 19, 2021;
Accepted manuscript posted November 30, 2021. doi:10.1115/1.4053217

Table 3 Statistical information of different slope/soil parameters

Slope/ Soil ID	Slope		Soil											
	Slope (°)		k_ϕ		k_c		B_n		$c\ (Pa)$		Φ (°)		$J\ (m)$	
	μ	σ	μ	σ	μ	σ	μ	σ	μ	σ	μ	σ	μ	σ
1	39	1	1×10^9	1000	5×10^8	500	2.8	0.01	950	1	37.5	0.5	0.048	0.001
2	36.5	1.5	5×10^8	1500	1×10^8	750	2.6	0.05	800	2.5	35	1	0.04	0.002
3	34.5	3	1×10^8	2000	5×10^7	2500	2.2	0.1	650	5	32.5	1.5	0.036	0.002
4	32	2.5	5×10^7	500	1×10^7	1500	2.2	0.02	500	10	30	1	0.032	0.003
5	26.5	2	1×10^7	1000	5×10^6	1000	2.0	0.1	450	15	27.5	2	0.029	0.002
6	17.5	1.5	5×10^6	2000	1×10^6	2000	1.8	0.01	300	5	25	0.5	0.024	0.001

* μ is the mean value, and σ is the standard deviation

Table 4 Comparison between different approaches for single vehicle path planning

Method	Situation	Length of the path	Calculation time (s)
Physarum	Original	48.19	0.66
	Dynamic-middle	98.21	0.94
	Dynamic-all	91.48	0.31
Dijkstra	Original	48.19	0.14
	Dynamic-middle	98.21	0.12
	Dynamic-all	91.48	0.12

Table 5 Comparison between different approaches for multi-vehicle path planning

Method	Situation	Overall length of all paths	Time of graph building (s)	Calculation time (s)
Physarum	Original	134.39	0.02	0.69
	Dynamic	173.85	0.02	0.59
Dijkstra	Original	134.39	0.01	1.06
	Dynamic	173.85	0.01	1.24

Journal of Mechanical Design. Received August 19, 2021;
Accepted manuscript posted November 30, 2021. doi:10.1115/1.4053217

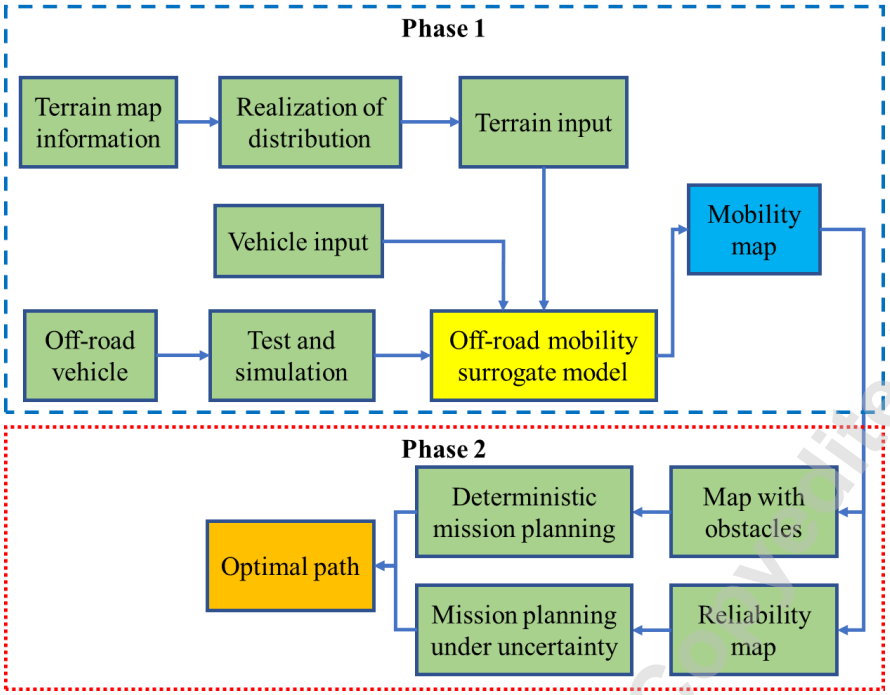

Figure 1 Process of mission planning for off-road vehicles

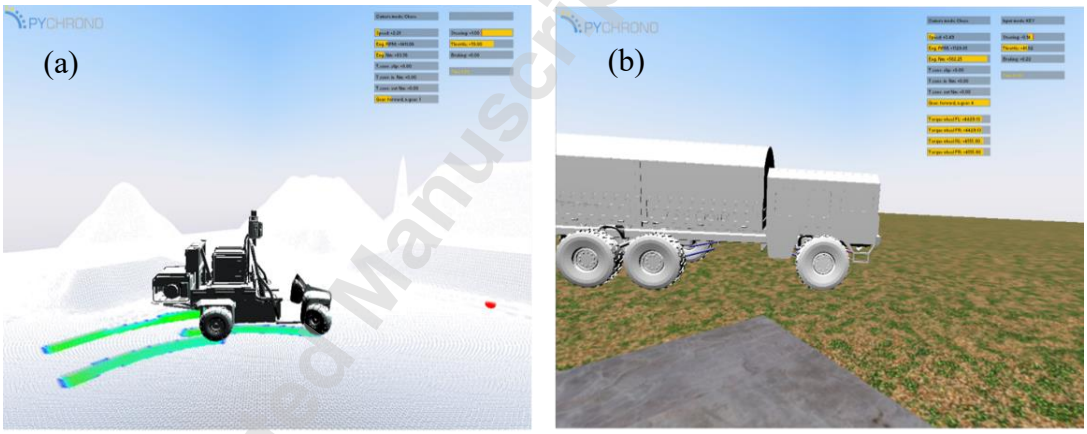

Figure 2 Two simulation examples of PyChrono: Vehicle: (a) gator UTV under deformable terrain, (b) MAN truck under rigid terrain.

Journal of Mechanical Design. Received August 19, 2021;
Accepted manuscript posted November 30, 2021. doi:10.1115/1.4053217

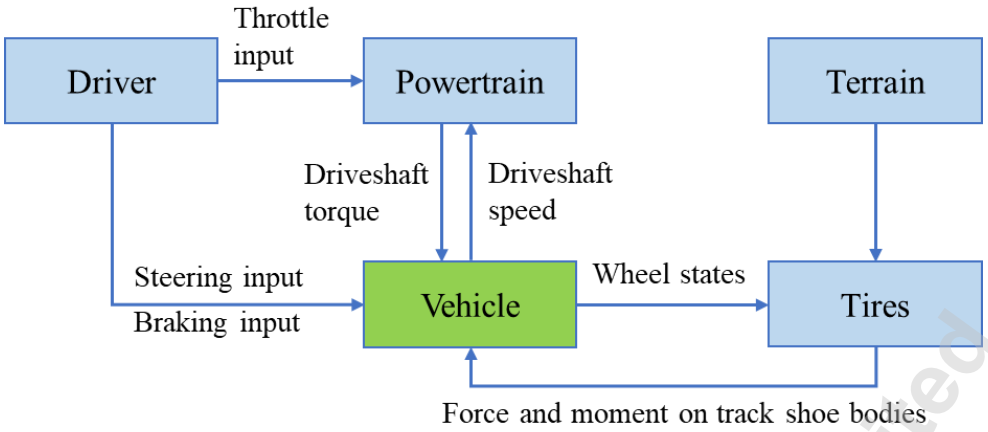

Figure 3 Simulation flowchart of PyChrono::Vehicle

(a) Hight map and path (b) Simulation running (c) Simulation output

Figure 4 A simulation model of off-road AGV in PyChrono

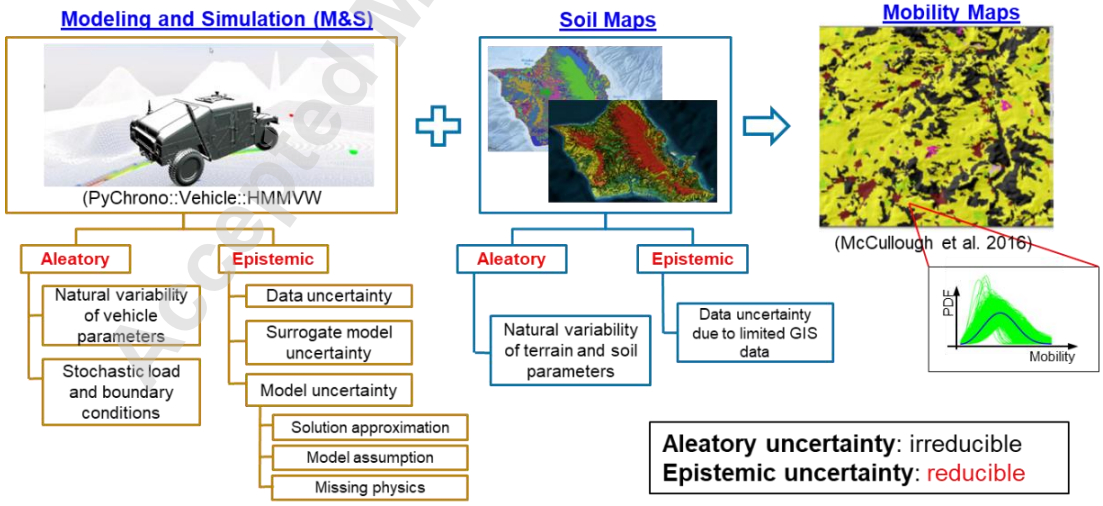

Figure 5 Uncertainty sources in terrain-related parameters

Journal of Mechanical Design. Received August 19, 2021;
Accepted manuscript posted November 30, 2021. doi:10.1115/1.4053217

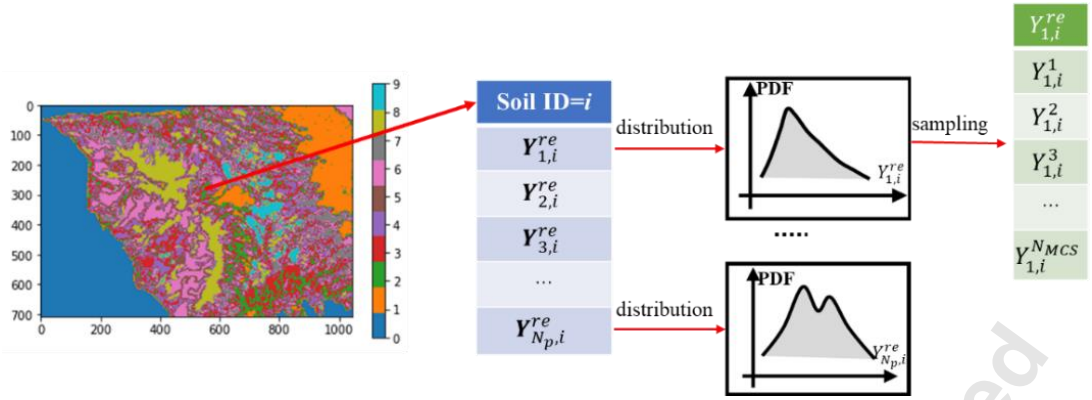

Figure 6 Uncertainty sources in terrain-related parameters

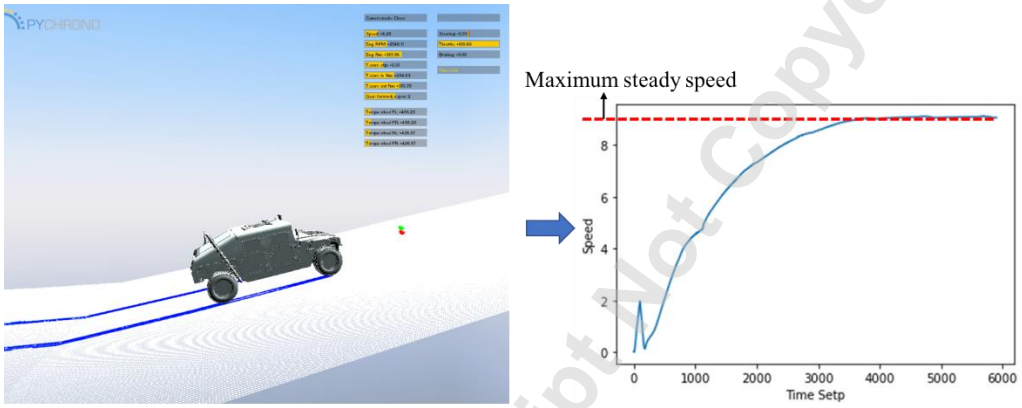

Figure 7 Vehicle mobility simulation model to predict the maximum attainable speed

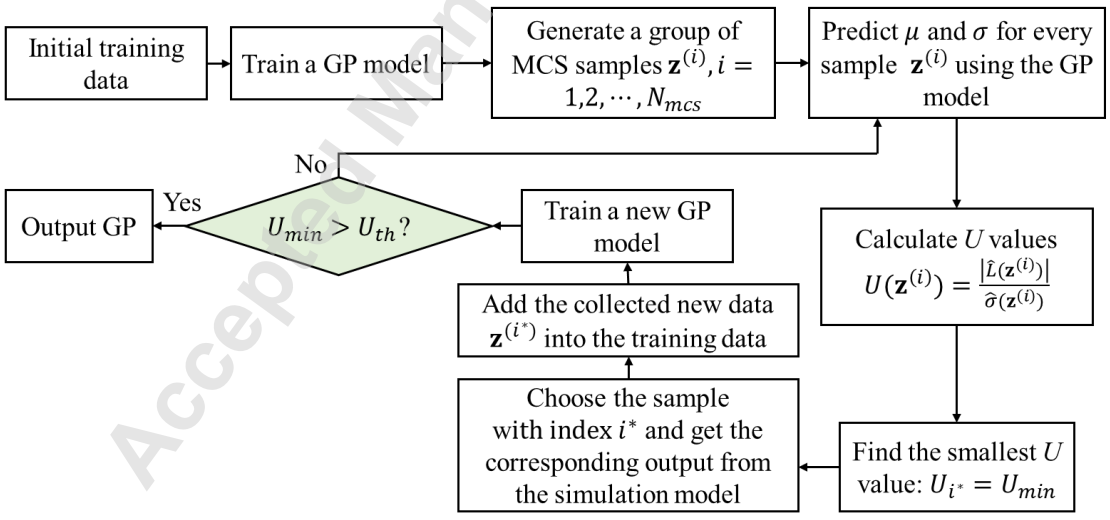

Figure 8 Flowchart of adaptive surrogate modeling-based reliability analysis

Journal of Mechanical Design. Received August 19, 2021;
Accepted manuscript posted November 30, 2021. doi:10.1115/1.4053217

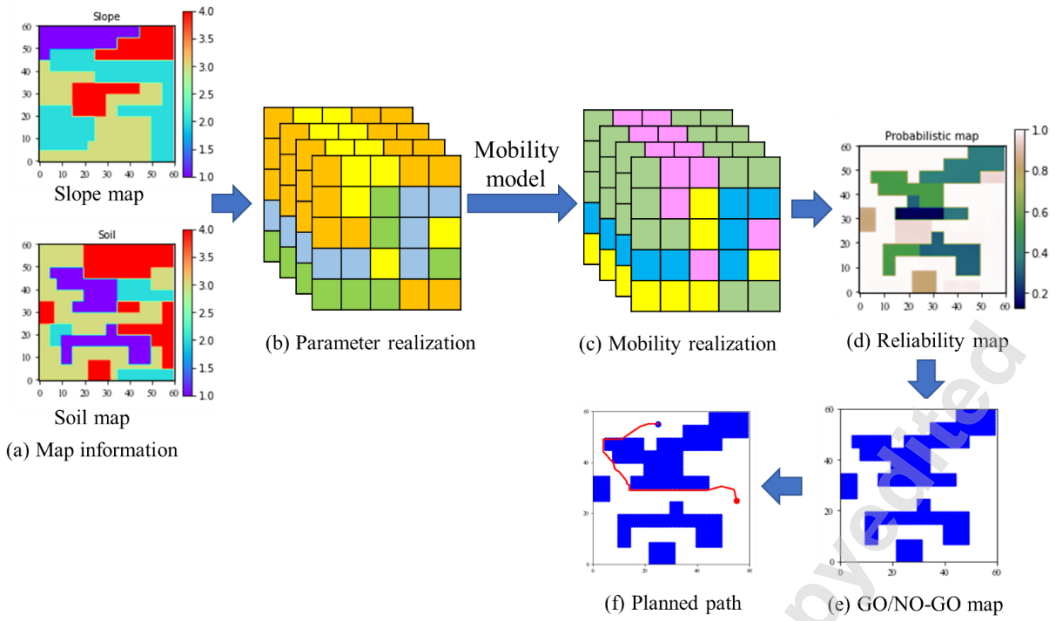

Figure 9 Flowchart of mobility reliability-based mission planning

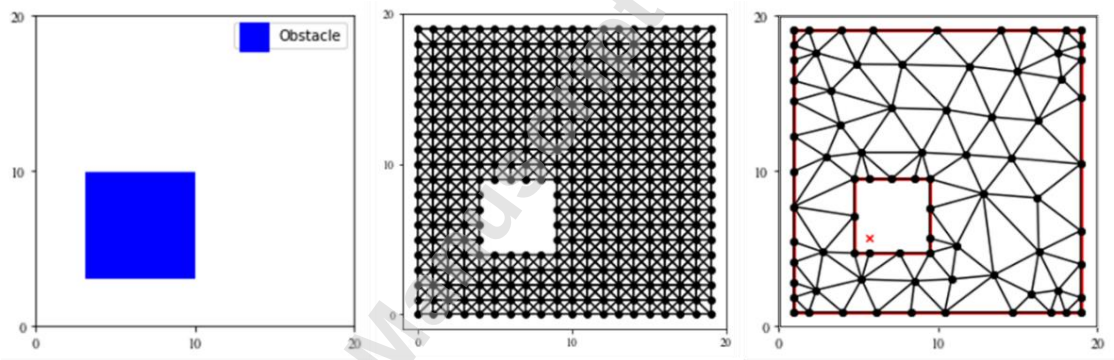

Figure 10 Comparison of uniform mesh and navigation mesh

Journal of Mechanical Design. Received August 19, 2021;
Accepted manuscript posted November 30, 2021. doi:10.1115/1.4053217

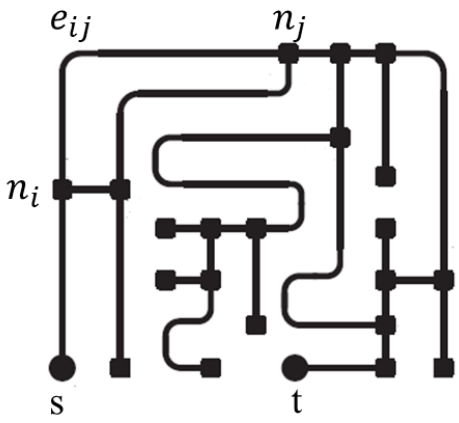

Figure 11 Graphical representation of the maze using a network

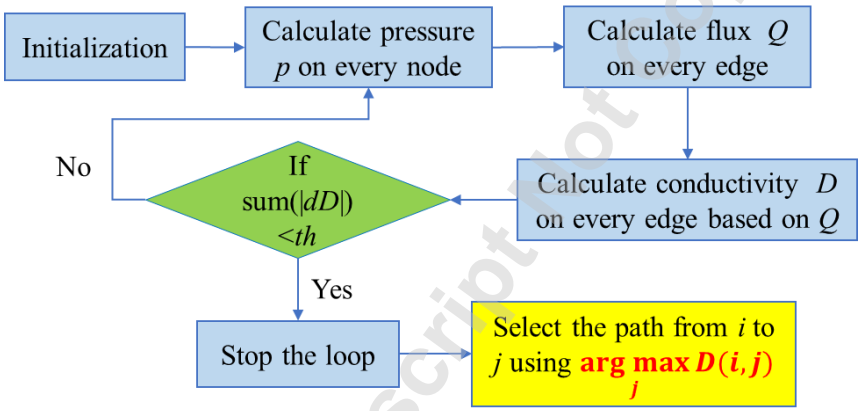

Figure 12 Flowchart of the Physarum solver algorithm

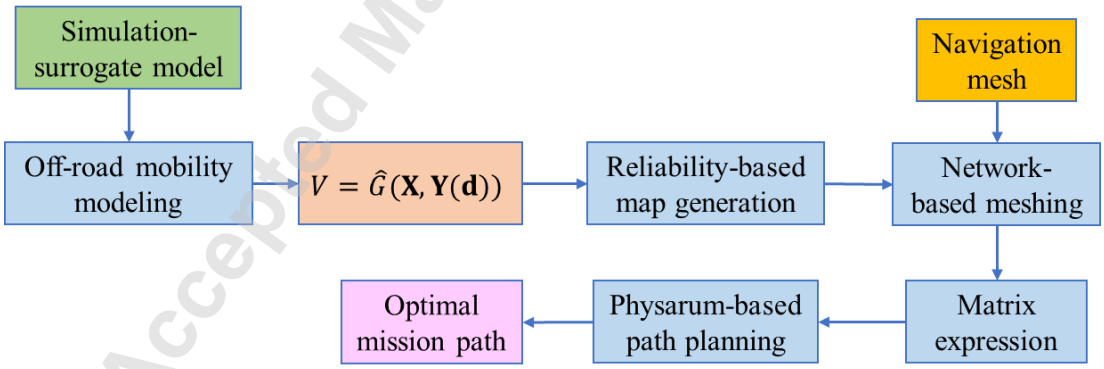

Figure 13 Flowchart of the proposed approach

Journal of Mechanical Design. Received August 19, 2021;
Accepted manuscript posted November 30, 2021. doi:10.1115/1.4053217

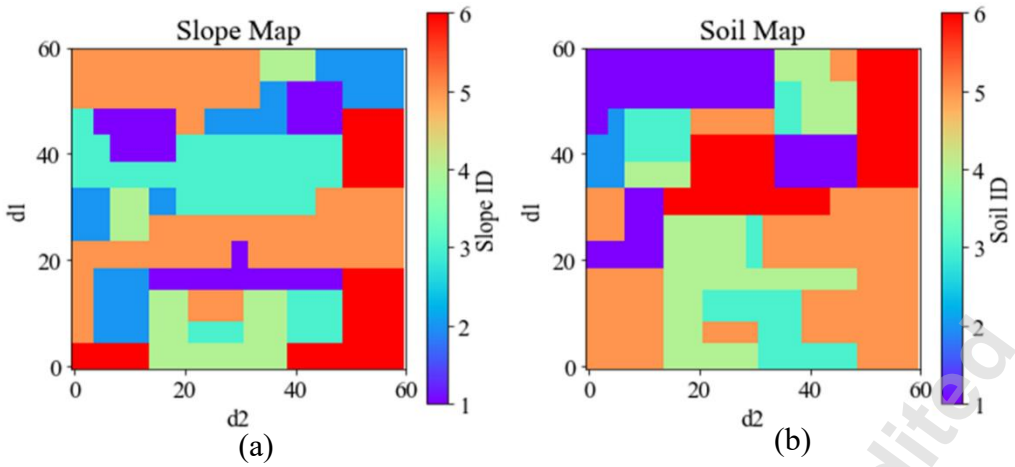

Figure 14 (a) Slope map and (b) Soil map of interest

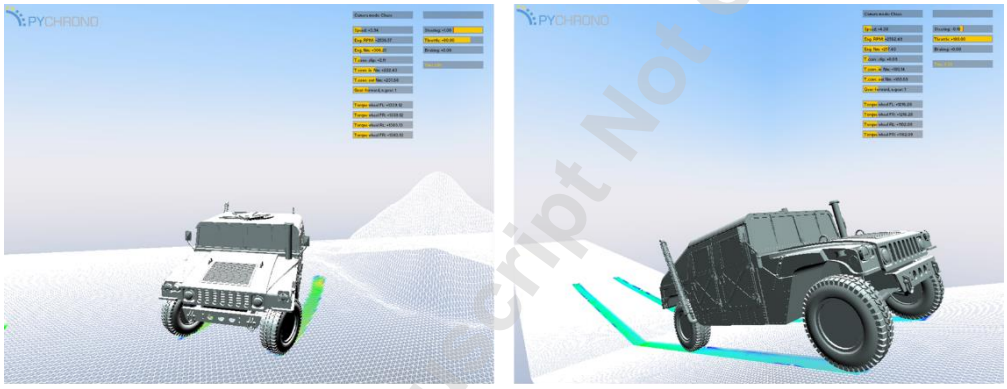

(a) Simulation for off-road environment (b) Simulation for hill climbing

Figure 15 HMMWV vehicle used in this numerical example

Journal of Mechanical Design. Received August 19, 2021;
Accepted manuscript posted November 30, 2021. doi:10.1115/1.4053217

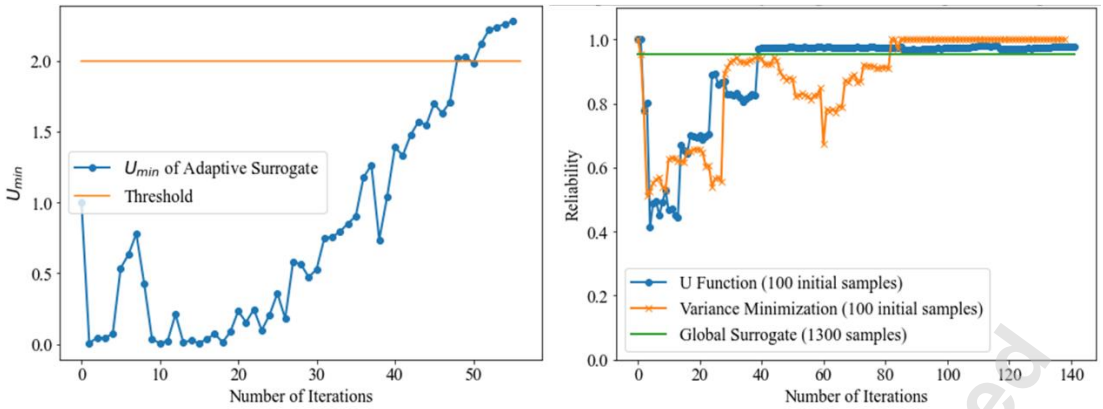

Figure 16 (a) Convergence history of $U_{\min}$ in adaptive surrogate modeling; (b) Convergence history comparison of adaptive surrogate modeling and the commonly used variance minimization-based surrogate modeling method

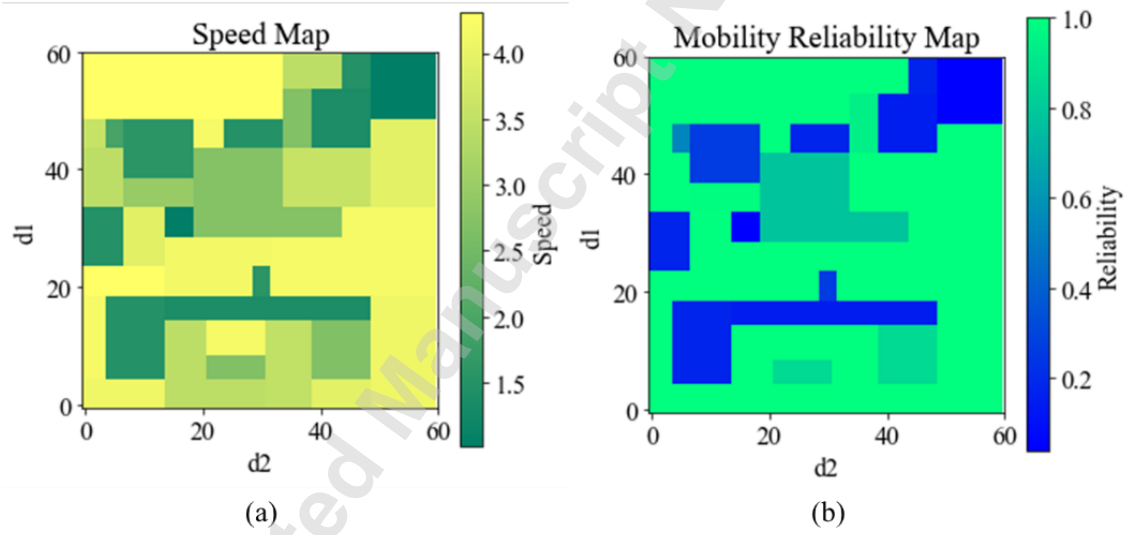

Figure 17 (a) Mean speed map and (b) SMR map

Journal of Mechanical Design. Received August 19, 2021;
Accepted manuscript posted November 30, 2021. doi:10.1115/1.4053217

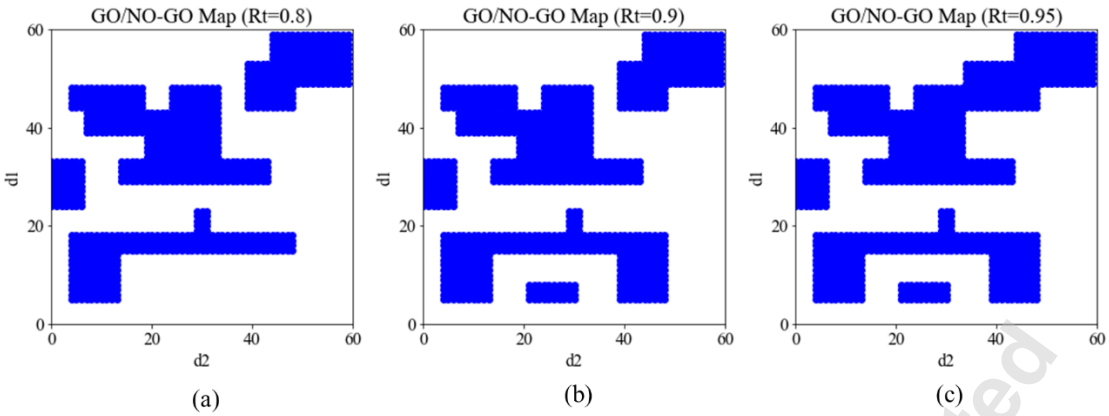

Figure 18 GO/NO-GO map (a) $R_t = 0.8$ (b) $R_t = 0.9$ and (c) $R_t = 0.95$

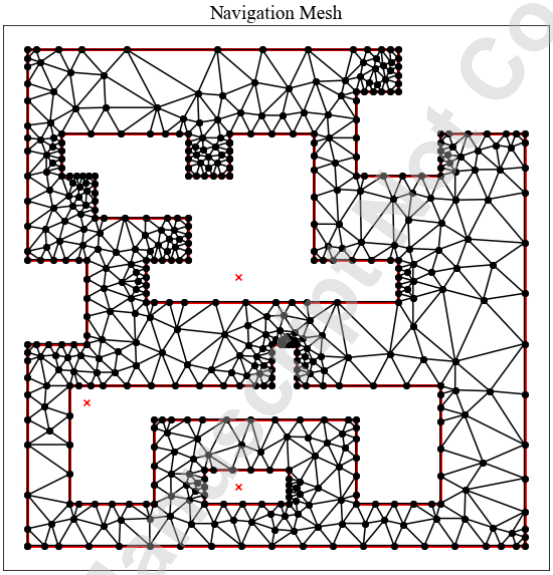

Figure 19 Navigation mesh of the map

Journal of Mechanical Design. Received August 19, 2021;
Accepted manuscript posted November 30, 2021. doi:10.1115/1.4053217

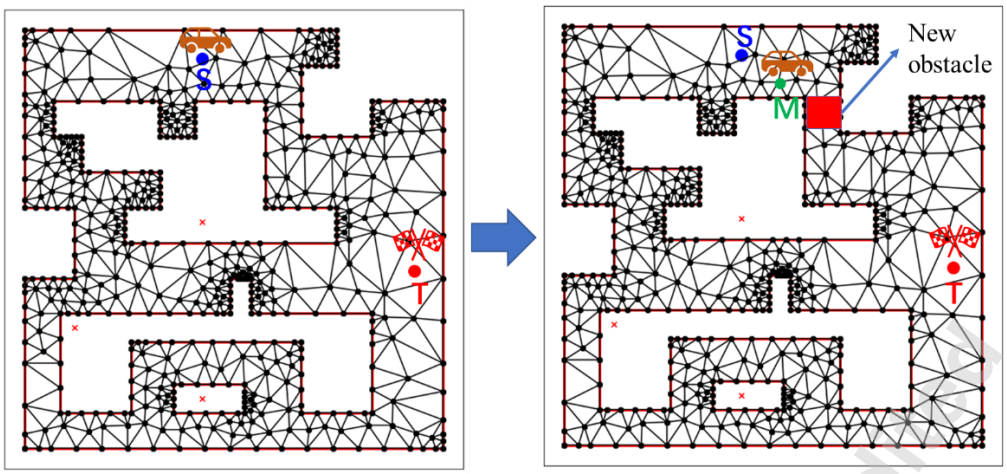

(a) (b)

Figure 20 (a) Original map and (b) Dynamic obstacle in the map

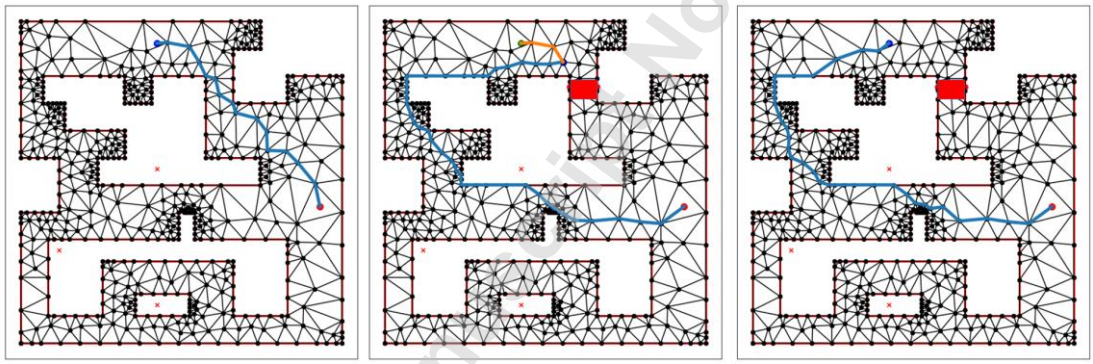

(a) (b) (c)

Figure 21 (a) Shortest path, (b) Dynamic path planning from the middle, and (c) Dynamic path planning from the starting point

Journal of Mechanical Design. Received August 19, 2021;
Accepted manuscript posted November 30, 2021. doi:10.1115/1.4053217

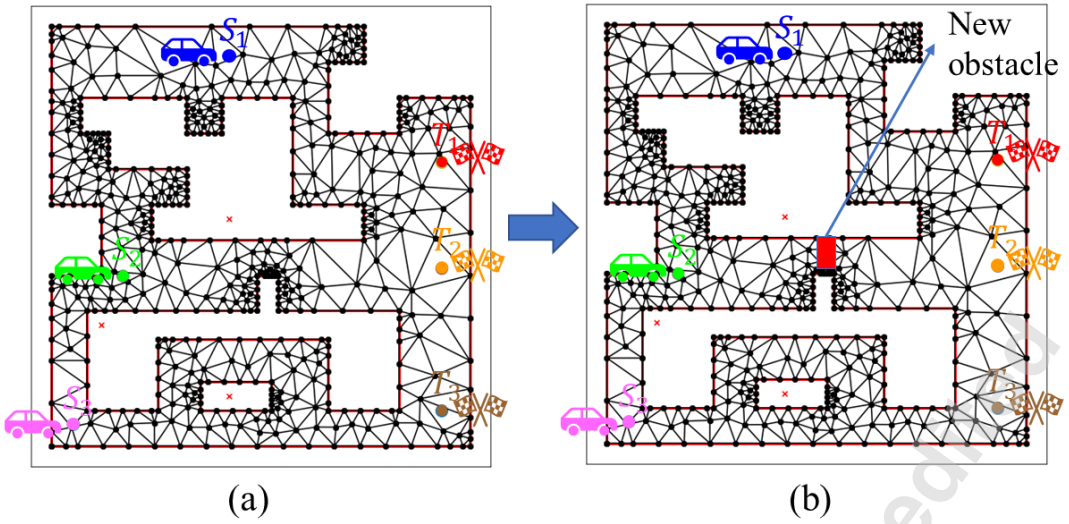

Figure 22 (a) Original map and (b) Dynamic obstacle of the map

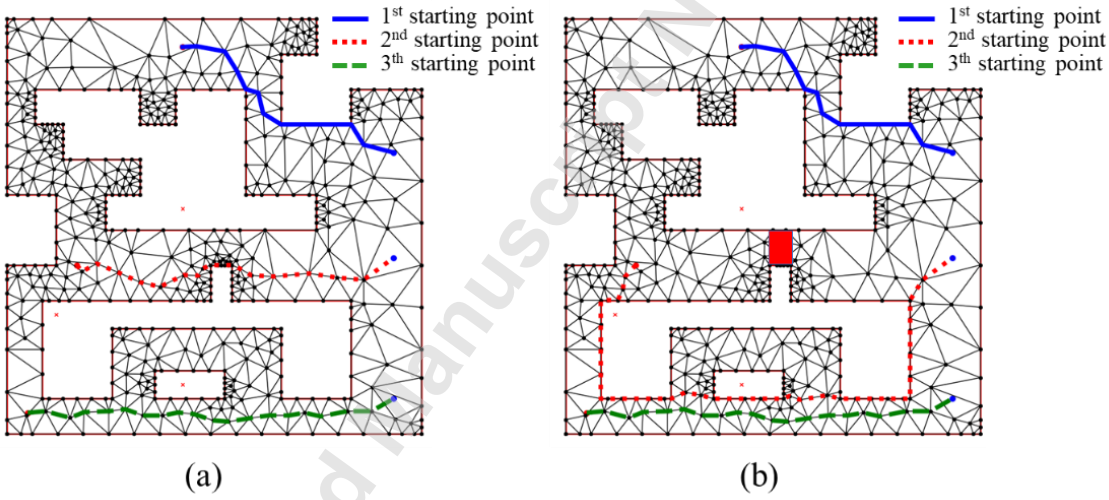

Figure 23 (a) original mission assignment and (b) dynamic mission assignment